

FINAL REPORT GR/T27280/01 ‘Opacity measurements at EUV wavelengths’

1. Introduction

Plasma-based extreme ultra-violet (EUV) lasers with saturated output at wavelengths as short as 5.9 nm were demonstrated by Tallents, Pert et al \approx 8 years ago. More recent work has shown that EUV pumping can be achieved with less than 1 J from the pump laser, opening up the prospect of applications requiring high average power. The grant (GR/T27280/01) reported here successfully demonstrated a new application where infra-red laser-irradiated targets are probed by the EUV laser beams in order to measure the opacity of plasma at densities and temperatures of relevance to laser-fusion and solar plasmas.. Depending on the design of the targets, plasma opacity at high densities and temperatures [1, 2, 3, 4] or the rate of laser ablation of solid target material [5, 6] has been measured. A comprehensive opacity modelling capability was built-up [7] and EUV lasers themselves were further developed [8, 9, 10, 11, 12, 13, 14]. The use of EUV lasers to measure laser ablation of solid targets was not outlined in the grant application, but was a successful ‘spin-off’.

We did not achieve measurements of opacity in targets heated by ‘hohlraums’ (black body cavities) or comparison with experimental broad-band backlighter opacity measurements as originally proposed. The risk with such experiments was high due to limited investment at the Central Laser Facility (CLF) on beamlines suitable for hohlraum heating or simultaneous backlighting (in addition to the beams to pump EUV lasing). Effort was shifted to ablation measurements where experiments were initially undertaken at the PALS laser Prague via EU access (LASERLAB) and later at the CLF. Some simulation work comparing broad-band and narrow frequency EUV laser opacity measurements was undertaken (see Huang PhD thesis and publications in preparation). We outline in the next two sections the opacity measurements and the ablation measurements. The work has been published in separate Physical Review Letter articles and other papers [1 – 7]. Development work on EUV lasers has also been published [8 – 14], with others in preparation. In total, three experiments of 6 weeks duration were undertaken at the CLF and two experiments on the PALS lasers. A comprehensive programme of theory and simulation work supported the interpretation of the experiments. A PhD thesis was awarded based on the work [15], with three others in preparation. We have published or are preparing for publication \approx 20 papers related to the grant work.

2. Opacity measurements

The opacity of material at extreme ultra-violet (EUV) photon energies is difficult to measure. Even the opacity of condensed aluminum which is often used as a radiation filter material is not known to high accuracy [16]. At high temperatures (> 1 eV) where materials are in the plasma state, there were some prior measurements of opacity in the EUV (photon energy 10 – 200 eV) [17, 18, 19]. However, it was not possible to make direct opacity measurements of near solid density materials at temperatures > 30 eV because background emission from the material overwhelmed the emission from the back-lighter used as the source of radiation for the measurement. Calculations using codes have been employed to understand the opacity of the sun, other astrophysical objects and laboratory plasmas. Examples of codes calculating plasma opacity include the Cassandra code [20], the opacity project calculations [21] and the Los Alamos code TOPS [22].

Figure 1 shows the configuration for an experiment undertaken at the CLF (now operated by STFC). The EUV laser output was imaged by a Mo-Si multi-layer mirror onto a sample target in order to measure the sample target opacity. The multi-layer mirror was positioned 86 cm from the EUV laser source to direct the beam to the opacity target, and focus it to an approximate diameter of 200 microns. A second spherical multi-layer mirror, positioned 36 cm downstream from the opacity target imaged the transmitted EUV laser light onto a back-thinned Andor CCD camera, located 6.8 meters away. Baffling was placed at appropriate points to prevent unwanted light reaching the detector which was filtered with aluminum and parylene-N, each between 100 and 300 microns thick. The relatively narrow band-width of the multi-layer mirrors (~ 0.8 nm) also helped to remove unwanted light from reaching the detector. 100 micron diameter alignment cross-wires were placed in front of the CCD detector and are clearly visible in the images obtained (see figure 2).

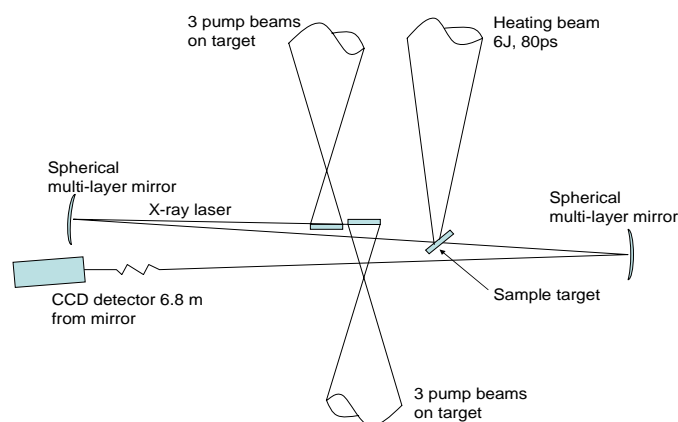


Figure 1 A schematic of the experiment. The 13.9 nm nickel-like silver EUV laser was pumped using a double target arrangement with each target irradiated by three 80 ps, 40 J beams focused to a line of length 22 mm and width 100 μ m. The EUV laser beam was focused to a diameter ~ 200 μ m onto the sample target by a spherical multi-layer mirror and this target separately heated by an 80 ps, 5 - 9 J beam, focused to a diameter of ~ 100 μ m. The EUV laser beam footprint at the sample target position was imaged onto a CCD detector by a second spherical multi-layer mirror.

The sample targets comprised a 50 (± 5) nm iron layer deposited on a 0.53 (± 0.05) micron parylene-N (CH) substrate and buried beneath an 80 (± 10) nm layer of parylene-N. The targets were orientated at 45 degrees to the EUV laser probe beam. Another $\sim 5 - 9$ J pulse of 80 ps duration from the VULCAN laser was focused to a spot of diameter 100 microns on the sample target in order to heat the iron layer. The sample targets were designed so that energy from the heating beam would be absorbed into the outer plastic layer, conductively heating the buried iron. This tamping slows down the rate of expansion of the iron layer to provide a plasma of improved uniformity and higher density. Radiative preheating of the buried layer can be ignored as the plastic top layer, once heated, is a weak emitter. Hot electron pre-heating at the employed irradiances ($\sim 10^{15}$ Wcm $^{-2}$) is also small.

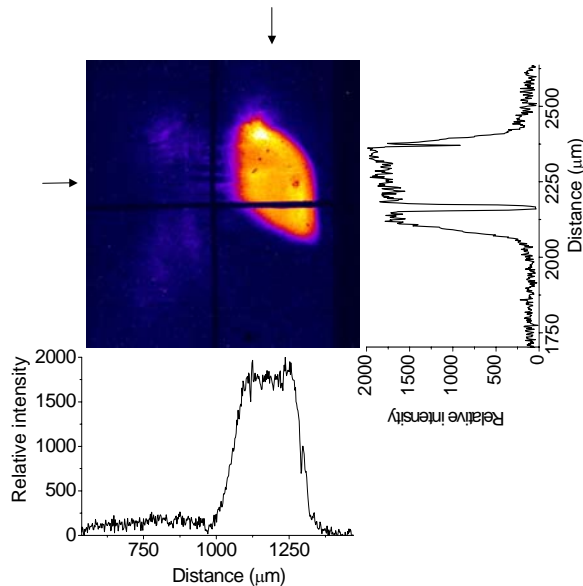


Figure 2 The footprint of the EUV laser as it passes through the opacity target at a time of 100 ps after the peak of the sample target irradiation. The brighter zone corresponds to an enhanced EUV transmission region where the target has been heated, whilst the most intense component of the EUV laser beam can be seen towards the left of the image passing through the unheated material. The central region of the heated region (as indicated by the intersection of the arrows) has been used to deduce the transmission of the heated target by comparison to transmission through unheated regions on the same shot.

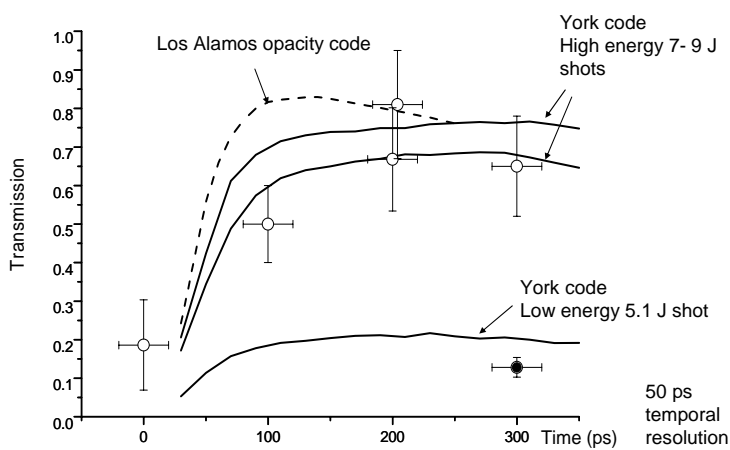


Figure 3 The variation of transmission of a 13.9 nm EUV laser with time from the peak of the heating pulse through the iron component of the sample target is shown for both experimental (data points) and simulated data (continuous curves). Experimental data with pulse energies in the range 8.4 – 9.2 J are shown as open circles, while a data point with pulse energy 5.1 J is shown as a filled in circle. Simulations are shown for heating laser energy of 6.5 J using the TOPS data (broken curve) and 7 - 9 J and 5.1J using our developed code (as labeled).

The opacity of the heated and high density iron was determined by measuring the transmission of the EUV laser beam through the sample target. Compared with the brightness of the EUV laser probe, the plasma self-emission was found to be negligible at ~ 100 counts compared with the peak transmission (~ 10000 counts) at the level of filtering used due to the unique

high brightness of the EUV laser. The arrival of the sample target heating beam was adjusted to enable probing of the plasma at different times in its evolution.

Figure 2 shows an example footprint of the EUV laser as it passes through the heated opacity target. The characteristic crescent shape [23] of the most intense part of the EUV laser beam is visible just to the left of the vertical cross-wire. A weaker, but more uniform part of the diverging EUV laser beam is transmitted strongly through the heated section and surrounding area of the sample target. This lower intensity, but more uniform component of the EUV laser beam has been used to make measurements of the transmission of the heated region by comparing the intensity of the EUV laser recorded in the heated section of the target to the intensity recorded on the same shot in the unheated section after allowance for the cold iron transmission (see figure 3). The error bars in the experimental points of figure 3 at 100 – 300 ps arise due to the uncertainty in the incident EUV laser intensity estimated for this procedure. The transmission is approximately constant towards the center of the heated target (see the cross-sections on figure 2) and the transmission measurements of figure 3 are from the central position.

We have made a measurement of the transmission of unheated targets by comparing the EUV laser transmission on different shots through the unheated sample target and through a filter of known transmission. This transmission measurement (0.19 ± 0.1) is plotted on figure 3 at time zero. The tabulated cold transmission of 50 (± 5) nm of iron is $0.083 (\pm 0.02)$ and so lies just within the estimated error. The measurement error is smaller ($\approx \pm 20\%$) for the heated target measurements as they are obtained in a single shot.

The transmission, T , of the sample target is related to the opacity (σ_i) of the different components of the target as a function of distance by

$$T = \exp\left(-\int \sqrt{2}\sigma_i\rho_i dx\right)$$

where ρ_i is the density variation of the sample target components and the integration is over the thickness of the sample target. The factor of $\sqrt{2}$ accounts for the 45 degree angle of incidence of the EUV laser beam to the sample target normal. The outer layer of plastic has been ignored in the analysis as its opacity contribution is low due to its untamped expansion (transmission > 0.75 for solid and close to unity once a plasma is formed). The transmission of the plastic substrate has been taken as its solid value throughout (transmission = 0.17). The 1.5D EHYBRID code [24] was used to model the variation of temperature and density with time for the expanding plasma of the sample target. Laser energies on target as for our experimental data (5.1 – 9.2 J) are employed for the simulations with an assumed reduction to 0.3 of these energies to allow for scatter and other processes (see Abou-Ali et al [25]) and an assumed energy dump of 30% at the critical density. The electron temperatures in the iron layer range from 30 eV (furthest from the laser) to temperatures in the range 250 eV (at 100 ps) to 150 eV (at 300 ps) closest to the laser, while the densities range from 0.2 – 0.008 gcm^{-3} (at 100 ps), 0.08 – 0.002 gcm^{-3} (at 200 ps) and 0.05 – 0.001 gcm^{-3} (at 300 ps). Two approaches have been employed to model the expected transmission through the iron layer. Tabulated multi-group opacity calculations from the Los Alamos opacity data TOPS were used to calculate the temporal development of the sample target iron opacity at the EUV laser wavelength (13.9 nm) by utilizing the temperature and density variation calculated from the EHYBRID code. A separate code was also developed to calculate the opacity directly from the EHYBRID predicted ionization, temperature and density and is outlined in the thesis of David Whittaker [45].

The TOPS opacities are determined assuming elemental abundances are in LTE. Inverse bremsstrahlung (free-free) contributions to the opacity are calculated from the Kramers cross-section formula and relativistic free-free-Gaunt factors. Photo-ionization (bound-free) contributions are calculated assuming populations given by the Saha equation and cross-sections calculated for $n \leq 5$, $\ell \leq 4$ using distorted wave Hartree-Fock calculations and hydrogen-like cross-sections for $n > 5$, $\ell > 4$. Our separate code follows the TOPS opacity evaluations for free-free and bound-free processes, but uses the EHYBRID time-dependent evaluations of the ionization balance. The bound-bound absorption of approximately 26000 tabulated transitions (listed in reference [21]) lying in the vicinity (over a 2.5 nm range) of the EUV laser wavelength are evaluated in our code. Collisional line broadening for the lineshape function is assumed. Line broadening is sufficiently large that there is little difference in the calculated opacities for our experimental conditions over the uncertainty range of the EUV laser wavelength (13.877 – 13.907 nm, see Li et al [26]).

The experimental transmission data is plotted with the simulation data superimposed in figure 3. The horizontal axis measures the delay between the peak of the heating pulse and the peak of the ≈ 40 ps duration EUV laser pulse arriving at the opacity target. The experimental data points were obtained with laser pulses pumping the EUV laser target in the range 30 J to 44 J, though because the EUV laser was saturated, the measured range of energies in the output EUV laser pulses was within $\pm 50\%$ of the mean. A range of laser energies irradiated the sample target (5 - 9 J) and this caused some of the range of transmissions seen for the EUV laser in figure 3. Good agreement can be seen between the experimental data points and modeling data at times of 100 and 200 ps with experimental pulse energies in the range 8.4 – 9.2 J. One of the measured transmissions at 300 ps is much lower than that predicted by the simulation with higher laser energies, but is in close agreement with our simulation at the reduced laser energy (5.1 J) corresponding to the energy of the 300 ps data point.

3. Ablation measurements

Mass ablation rates arising when lasers irradiate solid targets have been previously measured by recording the time of emission from buried signature layers in the targets [27, 28]. Ablation to the layer depth is said to be signalled by emission from the layer material, though such emission can also arise from an increase of electron temperature due to heat conduction without plasma expansion. Alternatively, mass ablation rates averaged over the laser pulse duration can be deduced from measurements of the total expanding plasma mass recorded from ion probe signals [29].

In an experiment undertaken at the PALS laser facility Prague, we temporally resolved laser ablation through thin targets of iron irradiated by an infra-red laser using the transmission of a soft EUV laser at 21.2 nm. Code calculations show

that ablated hot iron plasma is close to fully transparent and so the EUV laser transmission through an irradiated target is dominated by the absorption of the cold solid thickness of material not ablated. Our measurements differ from earlier studies with EUV laser pulses probing spatial variations in transmission through thick foils associated with the Rayleigh-Taylor instability [30,31]. In these earlier probing studies, variations in EUV laser transmission arose due to variations in opacity due to shock compression and areal density perturbations. These measurements also differ from the opacity measurements described above where a thin layer of iron in a target was tamped with plastic so that expansion was reduced, the iron was heated and the EUV transmission and hence opacity of the heated iron was measured.

The soft EUV laser at a wavelength of 21.2 nm arising from a 3p – 3s transition in Ne-like zinc was produced using the PALS infra-red (1.315 μm) laser operating with 480 ps duration output pulses. The EUV laser was created by irradiating a solid zinc target of length 3 cm with a low energy (< 2 J) pulse focussed to a 500 microns wide line, followed 10 ns later by the main pulse of 400 J, focussed to a line of width 100 μm . The long scale length pre-plasma with which the main pulse interacts provides good conditions for gain by reducing refraction effects, optimising the gain volume and maximising the absorption of the pump laser. To improve further the brightness, reproducibility and uniformity of the EUV laser beam, a half cavity mirror was installed and the re-injection point of the beam was tuned to drive the laser emission further into saturation. Operating well into laser saturation, the EUV laser output energy per pulse was reproducible to within $\pm 30\%$. Streak camera measurements indicate that the pulse duration of the EUV laser pulse is 90 - 130 ps. Our studies [9] have shown that the frequency bandwidth of EUV laser pulses is extremely narrow (such that $\Delta\nu/\nu < 10^{-4}$ and is more than an order-of-magnitude narrower than the bandwidth of individual absorbing lines in the probed plasma).

A near-normal incidence spherical multi-layer mirror focussed the EUV laser beam onto the sample target in a spot of 1 mm diameter at normal incidence. Another spherical multi-layer mirror imaged the sample target plane to a CCD detector so that the footprint of focussed EUV laser beam at the sample target was recorded with $6\times$ magnification and spatial resolution of 4 μm . The sample targets comprised 0.8 μm thickness of aluminium onto which was deposited a 50 nm thickness of iron. These targets were ablated using a third, separate 10 J, 480 ps laser pulse at 1.315 μm , focussed to a 120 μm full-width at half maximum diameter spot in the laser near-field with an approximately constant central spatial peak in irradiance (over 50 μm diameter). The variation in time of this peak irradiance is shown on figure 4. The transmission of the EUV laser pulse through the ablated target at the spatial position corresponding to the peak of the focussed infra-red irradiance (averaged over an area ≈ 30 μm diameter) was measured by comparing the recorded EUV laser flux with and without an ablated target on different shots. This enabled transmission measurements accurate to within approximately $\pm 30\%$, according to the reproducibility of the EUV laser from shot-to-shot. The time of arrival of the ablating laser pulse was adjusted relative to the other laser pulses producing the EUV laser and the relative timing measured with a Hamamatsu streak camera, allowing the sample target transmission and hence ablation to be probed in time (figure 4). Simulations predict that the EUV laser pulse peaks ≈ 100 ps before the peak of the 480 ps pump pulse. This shift in timing is allowed for in figure 4. The error in this 100 ps shift is small compared to the temporal resolution of the measurement (\approx EUV laser pulse duration $\approx 90 - 130$ ps).

As outlined in section 2, a code similar to the Los Alamos TOPS code, but with temperatures, densities and time-dependent (non-LTE) ionisation calculated by the Ehybrid fluid and atomic physics code has been developed at York under the grant. Our absorption calculations are more accurate than TOPS as we use the fluid code time-dependent ionization calculation and utilize the spectral position and oscillator strength of approximately 25000 lines tabulated by the Opacity Project with line widths calculated using a modified semi-empirical method assuming collisional broadening. At the high densities where significant EUV laser absorption occurs, the absorption predicted by our code is constant over the uncertainty range for the EUV laser wavelength (21.202 ± 0.01 nm) because of the large line broadening and high spectral density of absorbing lines. The predictions of the Ehybrid and opacity post-processor code for our experiment are superimposed on figure 4. There is some oscillation in the simulated transmission on figure 4 due to oscillations in the computed ionization abundance and continuum lowering, but the simulated transmissions follow the experimental results and a simple ablation model (described below).

Using our Ehybrid and opacity post-processor codes, we have examined EUV laser transmission,

$T = \exp\left(-\int \sigma \rho dx\right)$ as a function of distance x through our sample targets in order to check in more detail the switch-like nature of EUV laser transmission as ablation occurs. For example, at time 120 ps after peak irradiance, transmission through the expanding iron plasma ‘corona’ (here defined as density $\rho < 0.1$ gcm^{-3}) is 0.8. The transmissions through the ‘high density’ (7.86 $\text{gcm}^{-3} > \rho > 0.1$ gcm^{-3}) and solid ($\rho = 7.86$ gcm^{-3}) iron components are respectively 0.4 and 0.13. Our post-processor code calculations show that the opacity σ of ‘high density’ (7.86 $\text{gcm}^{-3} > \rho > 0.1$ gcm^{-3}) iron is comparable to the opacity of solid iron. For example, $\sigma = 6 \times 10^4$ cm^2g^{-1} for solid iron, while $\sigma \geq 10^4$ cm^2g^{-1} for iron of density 3 gcm^{-2} and temperature ≤ 50 eV.

Using deflagration and self-regulating models of ablation (see Pert [12]) and considering the experimentally measured variation of laser irradiance with time incident onto the sample target (see figure 4), we calculate the target material ablated as a function of time and evaluate the transmission of the EUV laser through the unablated target material using tabulated solid EUV transmissions (see model curves on figure 4). The deflagration and self-regulating models give different variations of the expected EUV laser transmission and it is clear that the self-regulating model is applicable for this experiment. To fit the data, absorption (A), of the laser energy is a free parameter and is shown in the range $A = 0.05 - 0.1$ on figure 4. Such a value is low compared to $A \approx 0.3$ measured for lasers of wavelength 1.06 μm , but A is expected to be smaller for the conditions of this experiment, namely a longer wavelength laser (1.315 μm).

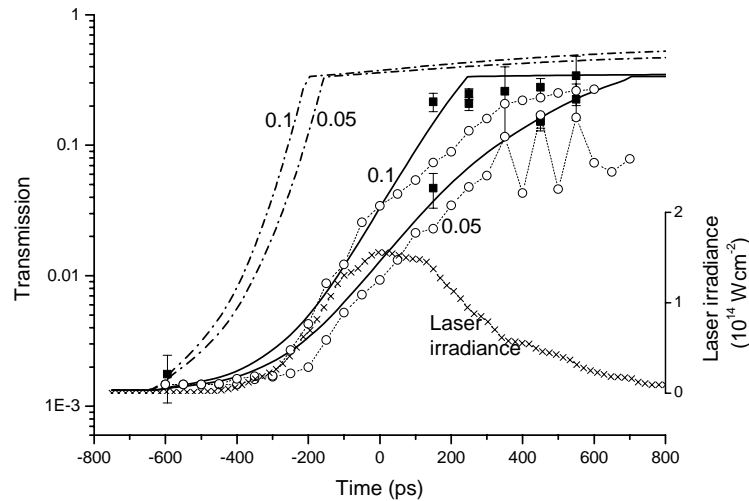


Figure 4 Data points (filled squares) show the measured transmission of 21.2 nm laser light through 50 nm of iron and 0.8 microns thick aluminium as a function of time from the peak of a laser pulse of irradiance variation as shown (x) ablating the iron layer. Simulations of the transmission using Ehybrid and a post-processor are shown as open circles with $A = 0.05$ or 0.1 (as labelled) absorption of the laser power. The solid and broken (dot-dash) curves are the transmission through unablated target material assuming ablation according to the deflagration model (broken curve) or self-regulating model (solid curve) with $A = 0.05$ or 0.1 (as labelled).

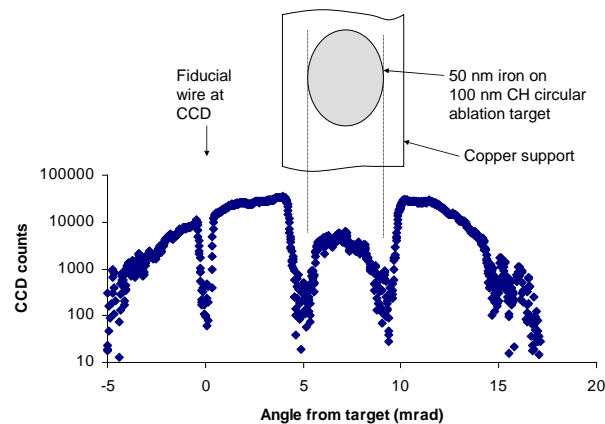


Figure 5 EUV laser profile at 13.9 nm after passing through a circular secondary target of 1 mm diameter comprising 50 nm Fe on 100 nm CH in a thick copper support. A flat field spectrometer records the angular variation of EUV output and clearly shows the attenuation due to the secondary target placed at 45° to the EUV laser beam (hence the elliptical appearance of the target to the beam). The iron was irradiated at up to $\approx 6 \times 10^{12} \text{ Wcm}^{-2}$ for 300 ps (FWHM) and this measurement was taken at the peak of the heating pulse in an experiment at the CLF (TAW 2007)

We have also made EUV laser transmission measurements similar to figure 4 for pure aluminium foils of $0.8 \mu\text{m}$ thickness ablated by 480 ps laser pulses. The transmission range is much narrower ($T = 0.31 - 0.75$) than for iron targets, but a self-regulating model of laser ablation again fits the experimental results. With aluminium, we could measure the EUV laser transmission more accurately by using the transmission through unablated target material to calibrate the incident EUV laser intensity for each individual shot. However, ablation rates can be determined with greater accuracy with material of high solid opacity such as iron, where, for example, for our experiment with 50 nm thickness of iron, we measure a transmission change due to ablation greater than two orders-of-magnitude.

4. Personnel and expenditure

Dr Matthew Edwards was employed on the grant for the full duration (1 October 2004 – 30 September 2007). Two students (Nicola Booth and Hu Huang) were in-post as project students for the period and are currently writing-up PhD theses. An overseas-funded student Zhai Zirong worked in the research area and is also writing-up his thesis. A PPARC funded student David Whittaker completed his PhD in 2007 on the modelling of opacity relevant to our experiments [15]. A DTA student (Pritesh Mistry) completed his thesis in 2005 on the development of the EUV laser. He used a fast streak camera to show the proximity of EUV laser pulses to the transform limit (see also [8, 9])

Two ANDOR soft EUV CCD cameras (along with appropriate computers for framestores/data analysis) were purchased as outlined in the grant application and used in experiments at the CLF and PALS. We found that it was possible to

make transmission measurements using a flat field spectrometer rather than multi-layer mirrors (see figure 5) and so our expenditure on multi-layer mirrors (classed as consumable items) was less than outlined in the application. Some of this consumable funding (£10K) was used to pay for repairs to one of the ANDOR CCD cameras as it developed a fault outside of the warranty period. Some other consumable funding was vired to pay for conference attendance (SPIE) and a visit to General Atomic/UCSD in August 2007 by Tallents, Pert and Edwards (approx. £7K) where results from the grant work were presented and discussed. We purchased a turbo-molecular pump and gate valve (cost £10K) for the local laser facility at York as outlined in our application and this was used in some training experiments by students. Technician Coulthard supported the local laser laboratory and manufactured a crystal spectrometer used in experiments at RAL. Technician Bramley supported the computational work of the project.

5. Conclusion

Opacity and ablation measurements using EUV laser transmission through infra-red irradiated targets have been made. We have shown that tamping targets with plastic or similar low-Z material enables the opacity of thin signature layers of material such as iron to be measured, while with untamped targets, EUV transmission records the rate of laser ablation of the solid target material. A comprehensive opacity simulation capability was developed based on the York Ehybrid fluid and atomic physics code. Approximately 20 publications have been published or are in preparation recording the output of the grant. A PhD directly on the opacity simulation work was awarded in 2007. Another PhD on EUV laser development was awarded in 2005. Three other PhD theses are in preparation.

¹ M H Edwards, D Whittaker, P Mistry, N Booth, G J Pert G J Tallents et al [14 authors] 2006 Phys. Rev. Lett. **97**, 03500. ‘Opacity measurements of a hot iron plasma using an EUV laser’.

² G J Tallents et al , 2005 SPIE **5919**, 17. ‘Hot dense plasma opacity measurements using EUV lasers’.

³ G J Tallents et al, 2005 3rd Intern. Conf. Superstrong fields in plasmas (Varenna) Ed. D Batani and M Lontano. p353-364. ‘Plasma based EUV lasers used for opacity and ablation rate measurements’

⁴ G J Tallents et al 2006 EUV lasers 2006 (Springer) Ed. P V Nickles and K A Janulewicz p445-454. ‘Plasma opacity and laser ablation measurements using EUV lasers’.

⁵ M H Edwards et al, Phys. Rev. Lett. **99**, 195002 (2007). Laser ablation rates measured using EUV laser transmission’.

⁶ M H Edwards et al, 2005 SPIE **5919**, 28. ‘Ablation rates of iron and aluminium measured using an EUV laser’.

⁷ D S Whitaker, M H Edwards and G J Tallents, High energy density physics **3**, 314.(2007) ‘Simulations and Experimental Determinations of Hot, Dense Iron Plasma Opacity at 89 eV’.

⁸ A Klisnick et al 2006 JQSRT **99**, pp. 370-380 ‘Experimental study of the temporal coherence and spectral profile of the 13.9 nm transient EUV laser’.

⁹ P Mistry, M Edwards and G J Tallents 2006 Phys. Rev. **A75**, 013818. ‘EUV laser pulses at the Fourier transform limit’.

¹⁰ H Huang and G J Tallents 2006 JQSRT 102/3, pp 425-431 ‘The output of amplified spontaneous emission lasers’.

¹¹ G J Pert 2006 Phys. Rev. **A73**, 033809 ‘Optimizing the performance of nickel-like collisionally pumped EUV lasers.’

¹² G J Pert 2007 Phys. Rev. **A75**, 023808 ‘Optimizing the performance of nickel-like collisionally pumped EUV lasersII’

¹³ G J Pert 2007 Phys. Rev. **A75**, 06814 ‘Optimizing the performance of nickel-like collisionally pumped EUV lasersIII’

¹⁴ G J Pert 2006 Phys. Rev. **E73**, 066401 ‘Recombination and population inversion in plasmas generated by tunnelling ionization.’; G J Pert 2007 Phys. Rev. **E76** 056404 ‘Population inversion in plasmas generated during recombination cascades’.

¹⁵ D S Whittaker, PhD thesis Univ. of York (2007) ‘Radiative opacity of dense iron plasma’.

¹⁶ R. Keenan, C. L. S. Lewis, J. S. Wark and E. Wolfrum J. Phys. **B35**, L447 (2002)

¹⁷ L. B. Da Silva *et al.*, Phys. Rev. Lett. **69**, 438 (1992).

¹⁸ C. Chenais-Popovics *et al.*, Astrophys. J. Suppl. **127**, 275 (2000).

¹⁹ J. M. Foster *et al.*, Phys. Rev. Lett. **67** 3255-3258 (1991).

²⁰ K. O’Nions, P. Pitman and C. Marsh, Nature **415**, 853 (2002)

²¹ M. J. Seaton, Y. Yan, D. Mihalas and A. K. Pradhan, Mon. Not. R. Astron. Soc. **266**, 805 (1994).

²² TOPS: A Multigroup Opacity Code; Los Alamos Report LA-10454, by Joseph Abdallah, Jr. and Robert E. H. Clark.

²³ G. J. Tallents J. Phys D: Appl. Phys. **36**, 259-276 (2003).

²⁴ G. J. Pert, J. Fluid Mech. **131**, 401 (1983)

²⁵ Y. Abou-Ali, Q. L. Dong, A. Demir, R. E. King, G. J. Pert and G. J. Tallents, J. Phys. B. **37** 2855 (2004).

²⁶ Y. Li, J. Nilsen, J. Dunn, A. L. Osterheld, A. Ryabtsev and S. Churilov, Phys. Rev. A **58**, R2668-R2671 (1998).

²⁷ J A Tarvin *et al.* Phys. Rev. Lett. **51**, 1355 (1983).

²⁸ P A Jaanimagi, J Delettrez, B L Henke and M C Richardson, Phys. Rev. **A34**, 1322 (1986).

²⁹ T J Goldsack, J D Kilkenny and P T Rumsby, J. Phys. **D14**, L47 (1981).

³⁰ E. Wolfrum et al 1998 Phys. Plasmas **5**, 227.

³¹ D. H. Kalantar *et al.*, Phys. Rev. Lett. **76**, 3574–3577 (1996).